J. Am. Soc. Mass Spectrom. (2016) 27:344–351
DOI: 10.1007/s13361-015-1291-y

RESEARCH ARTICLE

# Nonlinear Ion Harmonics in the Paul Trap with Added Octopole Field: Theoretical Characterization and New Insight into Nonlinear Resonance Effect

Caiqiao Xiong,[1] Xiaoyu Zhou,[1] Ning Zhang,[1] Lingpeng Zhan,[1] Yongtai Chen,[2] Zongxiu Nie[1,3]

[1]Beijing National Laboratory for Molecular Sciences, Key Laboratory of Analytical Chemistry for Living Biosystems, Institute of Chemistry, Chinese Academy of Sciences, Beijing, 100190, China
[2]School of Information Engineering, Wuhan University of Technology, Wuhan, 430070, China
[3]Beijing Center for Mass Spectrometry, Beijing, 100190, China

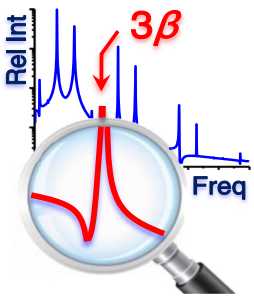


**Abstract.** The nonlinear harmonics within the ion motion are the fingerprint of the nonlinear fields. They are exclusively introduced by these nonlinear fields and are responsible to some specific nonlinear effects such as nonlinear resonance effect. In this article, the ion motion in the quadrupole field with a weak superimposed octopole component, described by the nonlinear Mathieu equation (NME), was studied by using the analytical harmonic balance (HB) method. Good accuracy of the HB method, which was comparable with that of the numerical fourth-order Runge-Kutta (4th RK), was achieved in the entire first stability region, except for the points at the stability boundary (i.e., β = 1) and at the nonlinear resonance condition (i.e., β = 0.5). Using the HB method, the nonlinear 3β harmonic series introduced by the octopole component and the resultant nonlinear resonance effect were characterized. At nonlinear resonance, obvious resonant peaks were observed in the nonlinear 3β series of ion motion, but were not found in the natural harmonics. In addition, both resonant excitation and absorption peaks could be observed, simultaneously. These are two unique features of the nonlinear resonance, distinguishing it from the normal resonance. Finally, an approximation equation was given to describe the corresponding working parameter, $q_{nr}$, at nonlinear resonance. This equation can help avoid the sensitivity degradation due to the operation of ion traps at the nonlinear resonance condition.

**Keywords:** Paul trap, Octopole field, Harmonic balance, Runge-Kutta, Nonlinear harmonics

Received: 2 July 2015/Revised: 23 August 2015/Accepted: 6 October 2015/Published Online: 23 October 2015

## Introduction

Quadrupole ion (Paul) trap, developed by Paul and Steinwedel in 1953 [1], has now been widely used as a mass analyzer in the mass spectrometry (MS) instruments. The ideal Paul trap should produce a linear quadrupole electric field. However, the electric field in the real trap always contains nonlinear higher-order field components, such as hexapole and octopole [2, 3]. Using the octopole field as an example, its typical weight regarding the field strength is ca. 1% due to the assembly misalignment and fabrication precision [4]. The weight can increase to 10% or higher in some Paul trap geometrical variations [5], such as cylindrical [6] and rectilinear ion traps [7]. The nonlinear fields inevitably introduce a series of nonlinear effects into the ion motion, such as frequency shift [8–10], amplitude variation [11], nonlinear resonance [12–16], and thus have great impacts on the trap performance, in terms of mass resolution [8], mass accuracy [9], sensitivity [12], and tandem MS (MS/MS) efficiency [10, 15], etc.

In the Paul trap, the ion motion consists of numerous harmonic motions, which can be clearly observed from the high-precision numerical frequency spectrum (Figure 1). Among the harmonics, the ones generated by the quadrupole field are

**Electronic supplementary material** The online version of this article (doi:10.1007/s13361-015-1291-y) contains supplementary material, which is available to authorized users.

*Correspondence to:* Caiqiao Xiong; *e-mail:* xiongcq@iccas.ac.cn, Zongxiu Nie; *e-mail:* znie@iccas.ac.cn

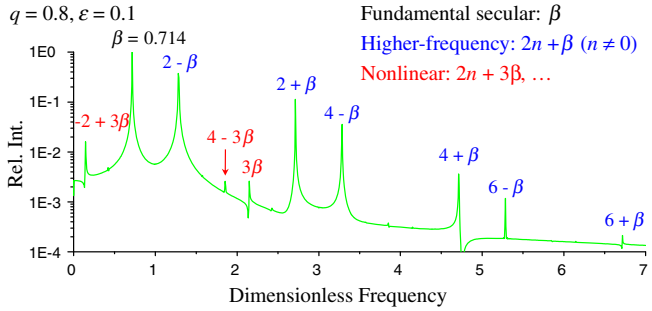


**Figure 1.** Frequency spectrum of ion motion at $a = 0$, $q = 0.8$, and $\varepsilon = 0.1$. The spectrum is obtained by using the fast Fourier transform (FFT) to the ion trajectory, which is calculated by the numerical fourth-order Runge-Kutta (4th RK) method. The fundamental secular, higher-frequency, and nonlinear frequencies of ion motion are marked by black, blue, and red colors, respectively. The initial displacement and velocity of the ion are set to 0.1 $r_0$ and 0, respectively. This initial condition is used throughout this article, unless otherwise specified

known as natural harmonics, including a fundamental secular oscillation (marked in black) and an infinite number of higher-frequency harmonics (marked in blue). The nonlinear fields make the ion motion even more complex. They not only change the frequencies and amplitudes of the natural harmonics but also produce nonlinear harmonics (marked in red) superimposed into the natural harmonics of ion motion [17, 18]. Generally, among the harmonics, the ion fundamental secular oscillation has the largest amplitude and is therefore the most important [2, 3]. By neglecting all the other small-amplitude harmonics, including higher-frequency and nonlinear ones, theoretical methods, such as the most often employed pseudo-potential well (PW) model [19, 20], can focus on the nonlinear effects of ion secular motion [10, 21–28].

The PW model can well describe the nonlinear frequency shift effect for Mathieu parameter, $q$, up to 0.8 with a typical error of less than 10% [10]. However, the PW model still suffers from some limitations because of the omission of the small-amplitude harmonics. The small-amplitude harmonics are closely related to the "fine structure" of the nonlinear effects [11]. For instance, in the PW method, the magnitudes of ion secular frequency shift, $|\Delta\beta|$, in the superimposed octopole fields, e.g., $\varepsilon = \pm 0.1$, are undistinguishable. But in the harmonic balance (HB) method, with the consideration of ion high-frequency harmonics, the $|\Delta\beta|$ at $\varepsilon = 0.1$ has been found to be greater than that at $\varepsilon = -0.1$. Herein, $\varepsilon = A_2/A_4$, $A_2$ and $A_4$ represent the dimensionless amplitudes of the quadrupole and octopole fields, respectively. In addition, the small-amplitude harmonics are important for the accuracy of the calculated ion trajectory in the nonlinear fields. For instance, regarding the calculated ion amplitude, the PW method can bring in an error of ca. 26% at $\varepsilon = 0.1$ and Mathieu parameter, $q = 0.6$. Under the same condition, the error decreases to ca. 2% in the HB method. Such accuracy is necessary for characterizing the nonlinear effects of ion motion because the typical ion amplitude variation is only ca. 5% of the ion amplitude.

Among the small-amplitude harmonics, the nonlinear harmonics of ion motion are especially interesting. First, they are the fingerprints of the nonlinear fields. For example, the octopole field mainly generates the characteristic 3β harmonic series (Figure 1) [17, 18]. From these characteristic harmonics, the detailed composition of the nonlinear fields in the trap can be readily determined. Second, the nonlinear harmonics of ion motion are the unique reason for the nonlinear resonance effect [12–16]. Depending on the corresponding types of the nonlinear harmonics, the nonlinear resonance can be classified into single-direction (i.e., $z$ or $r$ direction) and $r$-$z$ coupled resonances [16]. At nonlinear resonance, the natural and nonlinear harmonics match with each other, producing an effect of amplified ion amplitudes. This effect can give rise to possible ion losses and sensitivity degradation in the ion trap instruments. For instance, in the MS/MS experiments, the loss of daughter ions because of the nonlinear resonance has been knows as the black holes or black canyons [29]. But in the dipolar resonance experiments, the effect can accelerate the ion ejection and improve the mass resolution [30]. In addition, the nonlinear resonance may result in peak splitting effect in the quadrupole mass filter operated in the second stability region [31].

Theoretical characterization of the nonlinear harmonics of ion motion can shed light on the real ion motion in the nonlinear fields and help the design and optimization of the current high-performance instruments. However, the associated study has long been a challenge because the nonlinear harmonics are very weak in the ion motion and their typical amplitudes are 1% of ion secular harmonic or lower (Figure 1). In this article, taking advantage of the HB method, the ion motion in the quadrupole field with a superimposed weak octopole field was theoretically studied, in which the amplitudes, $D_{2n}$, and the frequencies, $2n + 3\beta$, of the nonlinear 3β harmonics series were calculated and the resultant nonlinear resonance effect at $\beta = 0.5$ was characterized.

## Theory

### *The Nonlinear Mathieu Equation (NME)*

Paul trap has a hyperbolic ring electrode and two hyperbolic endcap electrodes. To operate the trap, an electric voltage, $\Phi_0 = U - V\cos(\Omega t)$, is applied between the ring and the endcap electrodes [2, 3]. Herein, $U$ is the direct-current (DC) voltage, $V$ is the radio-frequency (rf) voltage with angular frequency $\Omega$, and $t$ is time. For a symmetric trap, the electric field only contains even multipole components, mainly including a quadrupole and a weak octopole [4]. The electric potential, $\Phi$, within the trap can be represented by:

$$\Phi = \Phi_0\left[A_2\left(\frac{r^2 - 2z^2}{2r_0^2}\right) + A_4\left(\frac{3r^4 - 24r^2z^2 + 8z^4}{8r_0^4}\right) + \ldots\right] \quad (1)$$

where $r$ and $z$ represent the radial and axial coordinates, respectively. The cross term, $-24r^2z^2$, of the octopole field can result in the coupling of ion motions in the $r$- and $z$-directions,

making the ion motion equation more difficult to solve analytically. For simplicity, only the ion motion along the *r*- and *z*-axis (i.e., $z = 0$ and $r = 0$, respectively) is considered, where the cross term vanishes and the ion motion is uncoupled. From Equation 1, it can be found that the electric potentials in the *r*- and *z*-directions have the same equation but different coefficients. Therefore, only the ion motion equation in the *z*- direction is solved as an example, considering that the ion ejection is operated in that direction. The ion motion in the *r*-direction can be studied by using exactly the same method.

The ion motion in the electric field can be described by the Newton's second law. Along the *z*-axis (i.e., $r = 0$), the ion motion equation yields:

$$m\frac{d^2z}{dt^2} = eE_z = -e\frac{\partial\Phi(r=0)}{\partial z} \tag{2}$$

where $m$ is ion mass, $e$ is electron charge, $t$ is time, $E_z$ is field strength of the electric field in the $z$ direction. Substituting the electric potential, $\Phi(r = 0)$ in Equation 1 into Equation 2, it yields:

$$\frac{d^2z}{d\xi^2} + [a_z - 2q_z\cos(2\xi)]\left(z + \frac{2}{r_0^2}\varepsilon z^3\right) = 0 \tag{3}$$

Equation 3 is the NME [17], in which $a_z$ and $q_z$ are dimensionless Mathieu parameters, $\xi$ is dimensionless time and they are defined as:

$$a_z = -\frac{8A_2eU}{mr_0^2\Omega^2} \tag{4}$$

$$q_z = -\frac{4A_2eV}{mr_0^2\Omega^2} \tag{5}$$

$$\xi = \frac{\Omega t}{2} \tag{6}$$

## *The Harmonic Balance (HB) Method*

Both theoretical methods and numerical methods can be utilized to solve the NME. Each sort of the methods has its own advantages and disadvantages. Generally, the numerical methods are more accurate, and their typical calculation error is ca. 1% of the ion amplitude. Hence, the numerical fourth-order Runge-Kutta (4th RK) is always utilized to determine the accuracy of the theoretical methods [32]. However, the theoretical methods can provide better understanding about the observed nonlinear effects. In order to keep the advantages simultaneously, it is highly desired that there is a theoretical method that is as accurate as the numerical methods.

The HB method is such a high-accuracy theoretical method [11]. In the HB method, a trial solution, which is the addition of ion motion harmonics, is employed and substituted into the NME. By balancing the coefficient of each harmonic, the amplitudes and the frequencies of all the harmonics can be obtained. The employed trial solution is important for the accuracy of the HB method. To accurately and systematically describe the nonlinear effect introduced by the superimposed octopole field, the trial solution should contain all the harmonics of ion motion, including the natural harmonics and the nonlinear harmonics. Regarding the octopole field, the nonlinear harmonics of ion motion mainly refer to the 3β harmonics series. Higher-order nonlinear harmonics, such as 5β and 7β series, are too small to be observed in the frequency spectrum (Figure 1). Hence, the trial solution of the HB method yields:

$$z(\xi) = \kappa'\sum_{n=-\infty}^{\infty}[C_{2n}\cos(2n+\beta)\xi + D_{2n}\cos(2n+3\beta)\xi] + \kappa''\sum_{n=-\infty}^{\infty}[C_{2n}\sin(2n+\beta)\xi + D_{2n}\sin(2n+3\beta)\xi] \tag{7}$$

where $\kappa'$ and $\kappa''$ are arbitrary constants, depending on the initial condition of the ion. $C_{2n}$ and $D_{2n}$ are the amplitudes of the natural harmonics and nonlinear harmonics, respectively. β is the frequency of the secular harmonic. $C_{2n}$, $D_{2n}$, and β can be exactly solved from $a_z$ and $q_z$. For an initial ion velocity of zero, the $\kappa''$ is equal to zero and the Equation 7 becomes:

$$z(\xi) = \kappa'\sum_{n=-\infty}^{\infty}[C_{2n}\cos(2n+\beta)\xi + D_{2n}\cos(2n+3\beta)\xi] \tag{8}$$

The non-zero initial ion velocities are discussed in "Introduction" in the Supporting Information.

Substituting Equation 8 into Equation 3, it yields ("Theory" in the Supporting Information):

$$\kappa'\sum_{n=-\infty}^{\infty}\left\{\begin{array}{l}\left\{\left[(2n+\beta)^2 - a\right]C_{2n} + qC_{2n\pm2} - \frac{\varepsilon}{2r_0^2}a\kappa'^2 Sum1 + \frac{\varepsilon}{2r_0^2}q\kappa'^2 Sum2\right\}\cos(2n+\beta) + \\ \left\{\left[(2n+3\beta)^2 - a\right]D_{2n} + qD_{2n\pm2} - \frac{\varepsilon}{2r_0^2}a\kappa'^2 Sum3 + \frac{\varepsilon}{2r_0^2}q\kappa'^2 Sum4\right\}\cos(2n+3\beta)\end{array}\right\} = 0 \tag{9}$$

where

$$Sum1 = \sum_{\substack{i+j-k=n,\\ i-j+k=n,\\ -i+j+k=n}} C_{2i}C_{2j}C_{2k} + 3\sum_{-i-j+k=n} C_{2i}C_{2j}D_{2k} + 3\sum_{\substack{i+j-k=n,\\ i-j+k=n}}^{\infty} C_{2i}D_{2j}D_{2k} \tag{10}$$

$$Sum2 = \sum_{\substack{i+j-k=n\pm1,\\ i-j+k=n\pm1,\\ -i+j+k=n\pm1}} C_{2i}C_{2j}C_{2k} + 3\sum_{-i-j+k=n\pm1} C_{2i}C_{2j}D_{2k} + 3\sum_{\substack{i+j-k=n\pm1,\\ i-j+k=n\pm1}}^{\infty} C_{2i}D_{2j}D_{2k} \tag{11}$$

$$Sum3 = \sum_{i+j+k=n} C_{2i}C_{2j}C_{2k} + 3\sum_{\substack{i-j+k=n,\\ -i+j+k=n}} C_{2i}C_{2j}D_{2k} + \sum_{\substack{i+j-k=n,\\ i-j+k=n,\\ -i+j+k=n}} D_{2i}D_{2j}D_{2k} \tag{12}$$

$$Sum4 = \sum_{i+j+k=n\pm1} C_{2i}C_{2j}C_{2k} + 3\sum_{\substack{i-j+k=n\pm1,\\ -i+j+k=n\pm1}} C_{2i}C_{2j}D_{2k} + \sum_{\substack{i+j-k=n\pm1,\\ i-j+k=n\pm1,\\ -i+j+k=n\pm1}} D_{2i}D_{2j}D_{2k} \tag{13}$$

The functions, such as $\sum_{\substack{g_1(i,j,k)=n,\\ g_2(i,j,k)=n}} f(i,j,k)$, are defined as

$$\sum_{\substack{g_1(i,j,k)=n,\\ g_2(i,j,k)=n}} f(i,j,k) = \sum_{g_1(i,j,k)=n} f(i,j,k) + \sum_{g_2(i,j,k)=n} f(i,j,k) \tag{14}$$

where $\sum_{g(i,j,k)=n} f(i,j,k)$ means the summation of $f(i, j, k)$ for all the $i$, $j$, and $k$, such that $g(i, j, k) = n$.

The Equation 9 can only be satisfied such that

$$\left[(2n+\beta)^2 - a\right]C_{2n} + qC_{2n\pm2} - \frac{\varepsilon}{2r_0^2}a\kappa'^2 Sum1 + \frac{\varepsilon}{2r_0^2}q\kappa'^2 Sum2 = 0$$

$$for\ -\infty < n < \infty \tag{15}$$

$$\left[(2n+3\beta)^2 - a\right]D_{2n} + qD_{2n\pm2} - \frac{\varepsilon}{2r_0^2}a\kappa'^2 Sum3 + \frac{\varepsilon}{2r_0^2}q\kappa'^2 Sum4 = 0$$

$$for\ -\infty < n < \infty \tag{16}$$

By solving Equations 15 and 16, the β, $C_{2n}/C_0$ ($n \neq 0$), and $D_{2n}/C_0$ can be obtained, and the NME is analytically solved. In this article, Equations 15 and 16 were solved by using the Gauss-Seidel relaxation method with a truncation to $C_{\pm8}$ and $D_{\pm8}$ (i.e., $n = \pm4$) [33]. It should be noted that the current HB method is inapplicable for instable ion motion, e.g., at the stability boundary, β = 1, and at the nonlinear resonance condition, β = 0.5. But the nonlinear resonance effect can still be observed from the stable ion motions in the vicinity of β = 0.5, e.g., β = 0.49 and 0.51.

## Results and Discussion

To illustrate the impact of the nonlinear harmonics in the ion motion, their amplitudes in comparison with those of ion secular motion, $D_{2n}/C_0$, were first calculated by using the HB method. In the nonlinear 3β harmonic series, the 3β and –2 + 3β harmonics have the largest amplitudes (Figure 1). As an example, their amplitudes, $D_0/C_0$ (black curve), and $D_{-2}/C_0$ (red curve), along the $q$-axis at $\varepsilon = 0.1$ and $\varepsilon = -0.1$, are shown in Figure 2a and b, respectively. The initial displacement and velocity of the ion were set to 0.1 $r_0$ and 0, respectively. This initial condition was used throughout this article, unless otherwise specified. From Figure 2, it can be found that for most $q$ values, the $D_0/C_0$ and $D_{-2}/C_0$ are very small, typically less than 1%, regardless of the polarity of the superimposed octopole field. However, obviously increased amplitudes can be observed at high $q$ values, e.g, $q > 0.8$, and at the nonlinear resonance condition, e.g., around β = 0.5 (or $q = 0.64$). Especially, the nonlinear –2 + 3β harmonic (red curve) can even achieve an amplitude greater than 10% of the ion secular motion (i.e., $D_{-2}/C_0 > 0.1$). The result indicates that at those $q$ values, the 3β harmonic series should have large impact on ion motion.

To confirm the assumption, the HB methods with and without (i.e., $D_{2n} = 0$) 3β harmonic series are employed. The ion trajectories at $q = 0.8$ and $q = 0.625$ (or β = 0.4931) with ε = 0.1, were calculated and shown in Figure 3a and b, respectively. The results with and without 3β series are represented by

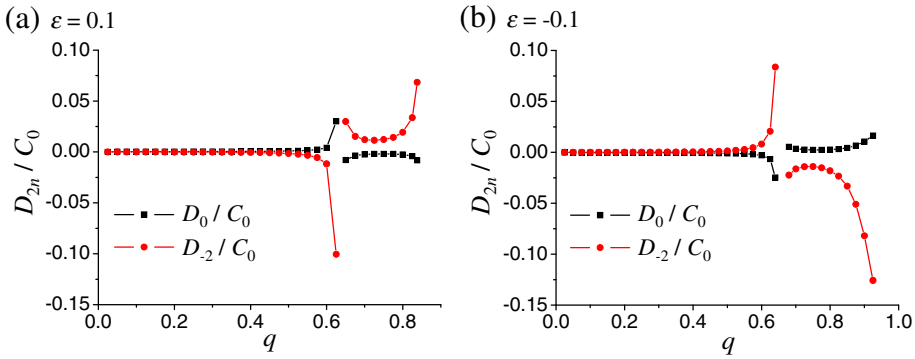


**Figure 2.** The amplitudes of ion nonlinear harmonics, $D_0/C_0$ (black curve) and $D_{-2}/C_0$ (red curve), as a function of $q$ at (a) $\varepsilon = 0.1$ and (b) $\varepsilon = -0.1$

the red and blue curves, respectively. As an accuracy standard, the numerical results calculated by the 4th RK method are also shown for comparison. From Figure 3c and d, enlarged plots of Figure 3a and b respectively, it is obvious that the HB method with 3β series (red curve) has significantly higher accuracy than that without 3β series (blue curve). Moreover, with 3β series, the analytical HB (red curve) and the numerical 4th RK results (black curve) are almost the same. This should not be a surprise because all the ion motion harmonics appearing in the numerical frequency spectrum (Figure 1) have now been fully considered in the HB method. To clearly show the influence of the 3β series, the ion trajectories contributed by the 3β series are extracted from Figure 3a and b and shown in Figure 3e and f, respectively. In Figure 3e, it can be found that at $q = 0.8$, all the harmonics in the 3β series together have an amplitude of 0.006 $r_0$ (red curve), which is ca. 1.5% of the ion trajectory amplitude, 0.4 $r_0$ (Figure 3a). However, the 3β series can introduce an error (i.e., $z_{diff} = z_{\mathrm{HB(without\ 3\beta\ series)}} - z_{\mathrm{HB(with\ 3\beta\ series)}}$) of 0.04 $r_0$ (or 10% of the ion trajectory amplitude) into the HB method (blue curve). This is because in the HB method, the 3β series has both direct (Equation 8) and indirect impacts (Equation 15) on the ion trajectory. Herein, the direct impact means that the 3β series, $D_{2n}$, itself is a composition of the ion trajectory amplitude. The indirect impact means that the $D_{2n}$ is also coupled with ion natural harmonics, $C_{2n}$. The result of Figure 3e indicates that even a small 3β series (e.g., 1.5%) may give rise to large calculation error (e.g., 10%) in the theoretical methods. In Figure 3f, it can be found that at around nonlinear resonance, $q = 0.625$, the amplitude of the 3β series, 0.02 $r_0$, is ca. 10% of the ion amplitude, 0.2 $r_0$ (Figure 3d). Therefore, it is not a surprise that neglecting such a large 3β series can produce the same large calculation error.

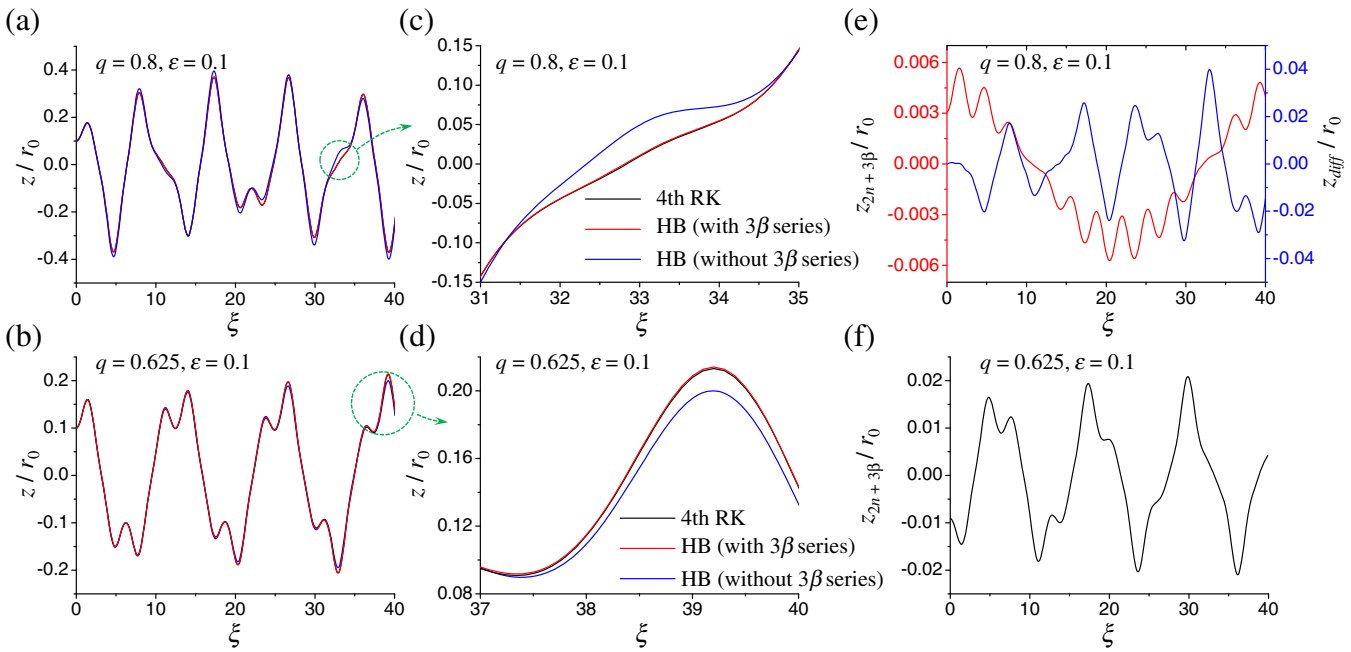


**Figure 3.** (**a**), (**b**) Ion displacement as a function of time $\xi$ at $\varepsilon = 0.1$, $a = 0$, (**a**) $q = 0.8$ and (**b**) $q = 0.625$ calculated by using the 4th RK method (black curve), the HB method with 3β series (red curve), and the HB method without 3β series (blue curve). (**c**), (**d**) Enlarged plots of (**a**) and (**b**), respectively. (**e**) Ion displacement of the 3β series, $z_{2n+3\beta}$, (red curve) and amplitude difference, $z_{diff}$, (blue curve) as a function of $\xi$ at $q = 0.8$. (**f**) $z_{2n+3\beta}$ as a function of $\xi$ at $q = 0.625$

Figure 4a and b show the maximum of ion trajectory amplitude, $z_{max}$, along the $q$-axis at $\varepsilon = 0.1$ and $\varepsilon = -0.1$, respectively. In Figure 4, it can be observed that the $z_{max}$ has an obvious resonant peak around the nonlinear resonance condition, $\beta = 0.5$ (green circle regions), where the resonant pairs of nonlinear harmonics and natural harmonics match with each other, e.g., $2 - 3\beta = \beta$. The increment of the maximum amplitude with the $q$ values can be attributed to the rf heating effect. To explore the underlying mechanism of the nonlinear resonance, the amplitudes of ion natural harmonics, $C_{-2}/C_0$ (black curve) and $C_2/C_0$ (red curve), at $\varepsilon = 0.1$ and $\varepsilon = -0.1$ are shown in Figure 4c and d, respectively. The ion secular frequency, $\beta$, at $\varepsilon = 0.1$ and $\varepsilon = -0.1$ are shown in Figure 4e and f, respectively. In Figure 4c–f, no resonant patterns can be observed in the natural harmonics with respect to the amplitudes (Figure 4c and d) and the frequencies (Figure 4e and f). Together with the results in Figure 2, it is obvious that it is the nonlinear $3\beta$ harmonic series alone that produces the nonlinear resonance effect. This phenomenon is dramatically different from that in the normal resonance. For example, in the dipolar resonance [34], when the frequencies of the ion secular motion and external AC excitation match with each other, both of them should have resonant peaks and they together produce the dipolar resonance.

To discover more interesting effects, the nonlinear resonances (green circle regions in Figure 4) under a series of different superimposed octopole fields were studied. Figure 5a shows the $z_{max}$ as a function of $q$ under positive superimposed octopole fields: $\varepsilon = 0.01$ (red curve), $\varepsilon = 0.05$ (blue curve), and $\varepsilon = 0.1$ (green curve). Figure 5b shows the $z_{max}$ as a function of $q$ under negative superimposed octopole fields: $\varepsilon = -0.01$ (red curve), $\varepsilon = -0.05$ (blue curve), and $\varepsilon = -0.1$ (green curve). The $z_{max}$ as a function of $q$ in the quadrupole field, $\varepsilon = 0$ (black curve) is also shown for comparison. In Figure 5, it can be observed that greater nonlinear resonant responses, $z_{max}$, can be observed at larger nonlinear field strengths, $|\varepsilon|$. This is because larger $|\varepsilon|$ can produce larger $3\beta$ series, $D_{2n}$, which plays a role of external excitation as in the dipolar resonance. Especially, it is interesting to find that nonlinear resonant excitation (i.e., increased amplitude compared with the background, $\varepsilon = 0$) and absorption peaks (i.e., decreased amplitude) can be observed in one spectrum, simultaneously. For instance, in the positive superimposed octopole fields (Figure 5a), the excitation and absorption peaks appear at $\beta < 0.5$ and $\beta > 0.5$, respectively. In the negative superimposed octopole fields (Figure 5b), the excitation and absorption peaks appear at $\beta > 0.5$ and $\beta < 0.5$, respectively. This is the second dramatic difference between the nonlinear and normal resonances. For the normal resonance, only one resonant pattern, either excitation or absorption, can be observed in one spectrum [34]. The ion excitation and de-excitation at nonlinear resonance can accelerate and delay the ion ejections in the dipolar resonance experiments [30]. In a linear ion trap, when the external AC frequency is scanned around the nonlinear resonance condition, simultaneous increment and decrement of the bandwidth of the frequency response profiles (FRP, i.e., ion ejection time versus the external AC frequency) have been observed.

The nonlinear resonance potentially gives rise to the ion loss and the sensitivity degradation of the ion trap instruments [12–16]. It is meaningful to predict the rf working voltage (represented by the $q$ value), at which the nonlinear resonance occurs. However, because of the frequency shift, the $q$ value at the nonlinear resonance condition (i.e., $\beta = 0.5$), $q_{nr}$, is also dependent on the superimposed octopole, $\varepsilon$, and the initial

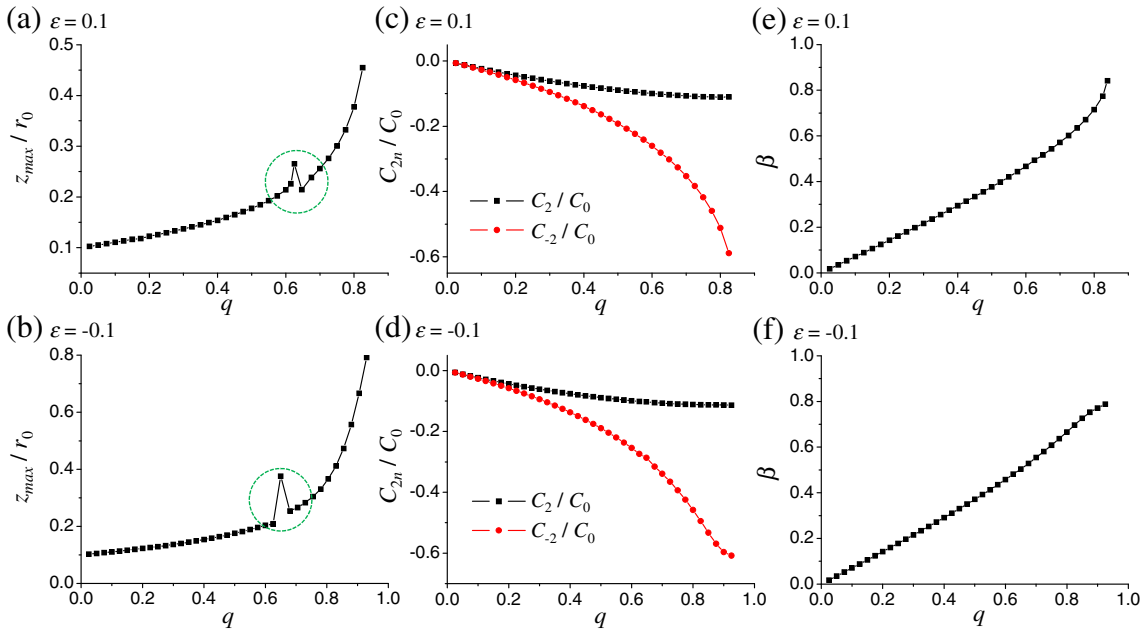


**Figure 4.** (**a**), (**b**) Ion amplitude, $z_{max}$, as a function of $q$ at (**a**) $\varepsilon = 0.1$ and (**b**) $\varepsilon = -0.1$. (**c**), (**d**) Amplitudes of ion natural harmonics, $C_2/C_0$ (black curve) and $C_{-2}/C_0$ (red curve), as a function of $q$ at (**c**) $\varepsilon = 0.1$ and (**d**) $\varepsilon = -0.1$. (**e**), (**f**) Ion secular frequency, $\beta$, as a function of $q$ at (**e**) $\varepsilon = 0.1$ and (**f**) $\varepsilon = -0.1$

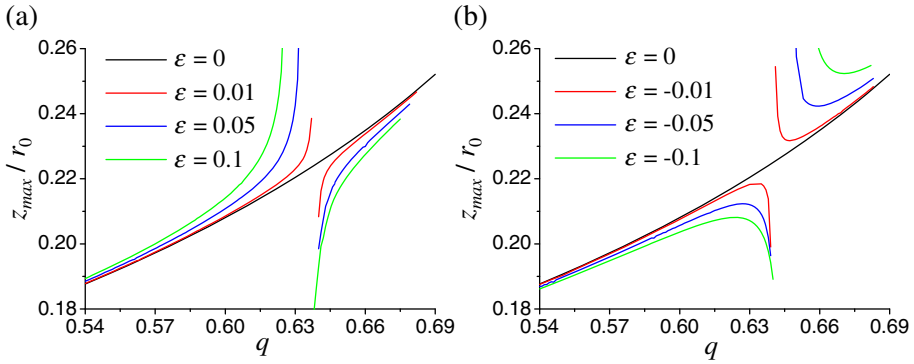


**Figure 5.** (**a**) Ion amplitude, $z_{max}$, as a function of $q$ in the positive superimposed octopole fields:, $\varepsilon = 0.01$ (red curve), $\varepsilon = 0.05$ (blue curve), and $\varepsilon = 0.1$ (green curve). (**b**) $z_{max}$ as a function of $q$ in the negative superimposed octopole fields: $\varepsilon = -0.01$ (red curve), $\varepsilon = -0.05$ (blue curve), and $\varepsilon = -0.1$ (green curve); $z_{max}$ as a function of $q$ in the quadrupole field, $\varepsilon = 0$ (black curve), is also shown for comparison

condition of the ion, $[z(0)/r_0]^2$ [17, 22, 26]. Figure 6a shows the β as a function of $q$ under positive superimposed octopole fields: $\varepsilon = 0.1$ (black curve), $\varepsilon = 0.05$ (red curve), and $\varepsilon = 0.01$ (blue curve). Figure 6b shows the β as a function of $q$ under negative superimposed octopole fields: $\varepsilon = -0.1$ (black curve), $\varepsilon = -0.05$ (red curve), and $\varepsilon = -0.01$ (blue curve). From Figure 6a and b, it can be observed that around β = 0.5, the β and $q$ values have good linear correlation. As a result, even if the HB method is inapplicable at β = 0.5, the $q_{nr}$ can be obtained by the linear fitting from its adjacent values between β = 0.49 and β = 0.51 (inset of Figure 6a). Using the method, the $q_{nr}$ at different $\varepsilon$ and $[z(0)/r_0]^2$ were calculated. Figure 6c shows the $q_{nr}$ as a function of $\varepsilon$ at $z(0) = 0.1\ r_0$. Figure 6d shows the $q_{nr}$ as a function of $[z(0)/r_0]^2$ at $\varepsilon = 0.1$. It can be found that the $q_{nr}$ has good linearity with the $\varepsilon$ (Figure 6c) and $[z(0)/r_0]^2$ (Figure 6d). As a result, the $q_{nr}$ can be conveniently evaluated by using an approximation equation, which yields:

$$q_{nr} = q_{nr0}\left[1 - \frac{\alpha}{r_0^2}\varepsilon z^2(0)\right] \tag{17}$$

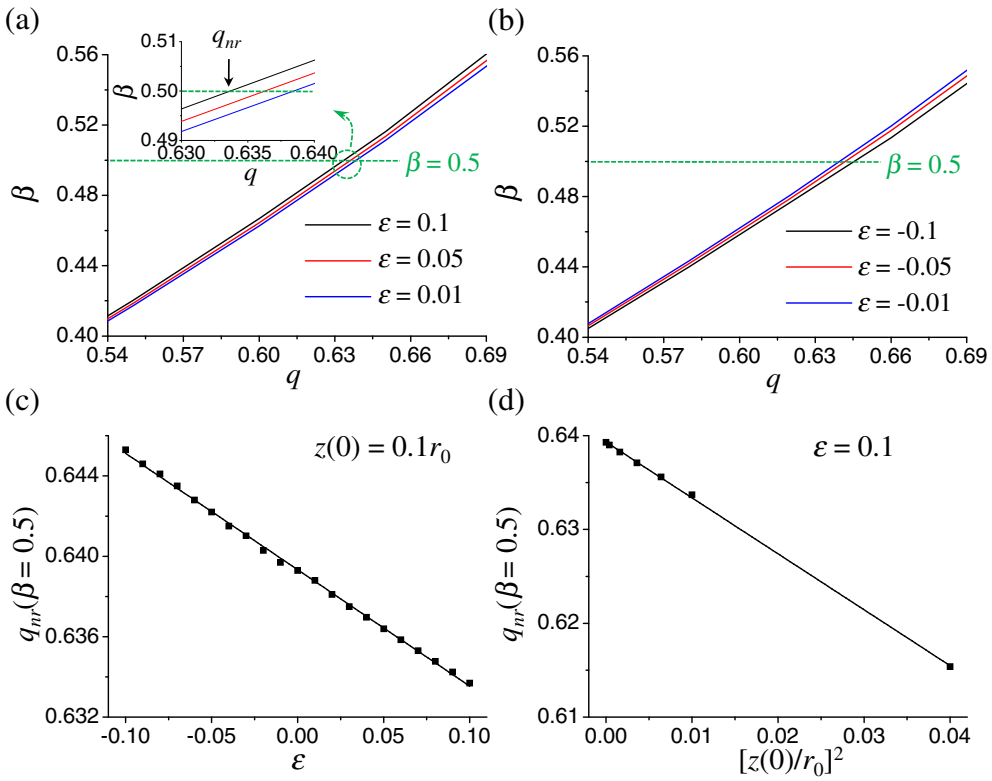


**Figure 6.** (**a**) Secular frequency, β, as a function of $q$ in the positive superimposed octopole fields: $\varepsilon = 0.01$ (blue curve), $\varepsilon = 0.05$ (red curve), and $\varepsilon = 0.1$ (black curve). The inset is an enlarged plot showing the $q_{nr}$ at nonlinear resonance condition, β = 0.5. (**b**) β as a function of $q$ in the negative superimposed octopole fields: $\varepsilon = -0.01$ (blue curve), $\varepsilon = -0.05$ (red curve), and $\varepsilon = -0.1$ (black curve). (**c**) $q_{nr}$ as a function of $\varepsilon$ at initial ion amplitude, $z(0) = 0.1\ r_0$. (**d**) $q_{nr}$ as a function of $[z(0)/r_0]^2$ at $\varepsilon = 0.1$

where $q_{nr0} = 0.6393$ is the $q_{nr}$ at $\varepsilon = 0$, and $\alpha \approx 9.1$ is the slope of the linear fitting (Figure 6c and d). The Equation 17 can help predict the nonlinear resonance conditions in various practical ion trap operations, and thus avoid the possible sensitivity degradation in the ion trap experiments.

## Conclusion

The HB method is a high-accuracy theoretical tool for characterizing the nonlinear effects in the Paul trap. For an ion in the quadrupole field with superimposed octopole field, its nonlinear harmonic motions and the perturbed natural harmonic motions are mutually coupled (Equations 15 and 16). Without the consideration of nonlinear harmonics, the real ion motion or the individual natural harmonic motions cannot be accurately obtained. The nonlinear harmonics give rise to the nonlinear resonance effect at $\beta = 0.5$, when they match with the natural harmonics, e.g., $2 - 3\beta = \beta$. At nonlinear resonance, it is the nonlinear ion harmonics that contribute to the nonlinear resonance effect, not the natural ion harmonics. Both the excitation and absorption peaks can be observed at the two sides of $\beta = 0.5$, simultaneously. The peak's position (i.e., at $\beta > 0.5$ or $\beta < 0.5$) is determined by the polarity of the superimposed octopole field. The rf voltages, $q$, at $\beta = 0.5$ in various ion trap experimental conditions are also given in Equation 17.

## Acknowledgments

The authors acknowledge support for this work by grants from the National Natural Sciences Foundation of China (grants no. 21175139, 21305144, 21475139, 21205123, 21321003, and 21127901), and the Chinese Academy of Sciences.

## References

1. Paul, W., Steinwedel, H.: A new mass spectrometer without a magnetic field. Z. Naturforsch. **8A**, 448–450 (1953)
2. Dawson, P.H.: Quadrupole mass analyzers: performance, design, and some recent applications. Mass Spectrom. Rev. **5**, 1–37 (1986)
3. March, R.E.: An introduction to quadrupole ion trap mass spectrometry. J. Mass Spectrom. **32**, 351–369 (1997)
4. Beaty, E.C.: Calculated electrostatic properties of ion traps. Phys. Rev. A. **33**, 3645–3656 (1986)
5. March, R.E., Todd, J.F.J.: Radio frequency quadrupole technology: evolution and contributions to mass spectrometry. Int. J. Mass Spectrom. **377**, 316–328 (2015)
6. Wells, J.M., Badman, E.R., Cooks, R.G.: A quadrupole ion trap with cylindrical geometry operated in the mass-selective instability mode. Anal. Chem. **70**, 438–444 (1998)
7. Ouyang, Z., Wu, G., Song, Y., Li, H., Plass, W.R., Cooks, R.G.: Rectilinear ion trap: concepts, calculations, and analytical performance of a new mass analyzer. Anal. Chem. **76**, 4595–4605 (2004)
8. Moradian, A., Douglas, D.J.: Mass selective axial ion ejection from linear quadrupoles with added octopole fields. J. Am. Soc. Mass Spectrom. **19**, 270–280 (2008)
9. Wells, J.M., Plass, W.R., Patterson, G.E., Ouyang, Z., Badman, E.R., Cooks, R.G.: Chemical mass shifts in ion trap mass spectrometry: experiments and simulations. Anal. Chem. **71**, 3405–3415 (1999)
10. Michaud, A.L., Frank, A.J., Ding, C., Zhao, X., Douglas, D.J.: Ion excitation in a linear quadrupole ion trap with an added octopole field. J. Am. Soc. Mass Spectrom. **16**, 835–849 (2005)
11. Xiong, C., Zhou, X., Zhang, N., Zhan, L., Chen, Y., Chen, S., Nie, Z.: A theoretical method for characterizing nonlinear effects in Paul traps with added octopole field. J. Am. Soc. Mass Spectrom. **26**, 1338–1348 (2015)
12. Dawson, P.H., Whetten, N.R.: Nonlinear resonances in quadrupole mass spectrometers due to imperfect fields I. The quadrupole ion trap. Int. J. Mass Spectrom. Ion Phys. **2**, 45–59 (1969)
13. Wang, Y., Franzen, J., Wanczek, K.P.: The nonlinear resonance ion trap. Part 2. A general theoretical analysis. Int. J. Mass Spectrom. Ion Processes **124**, 125–144 (1993)
14. Eades, D.M., Johnson, J.V., Yost, R.A.: Nonlinear resonance effects during ion storage in a quadrupole ion trap. J. Am. Soc. Mass Spectrom. **4**, 917–929 (1993)
15. Franzen, J.: The nonlinear ion trap. Part 5. Nature of nonlinear resonances and resonant ion ejection. Int. J. Mass Spectrom. Ion Processes **130**, 15–40 (1994)
16. Zhou, X., Xiong, C., Zhang, S., Zhang, N., Nie, Z.: Study of nonlinear resonance effect in Paul trap. J. Am. Soc. Mass Spectrom. **24**, 794–800 (2013)
17. Zhou, X., Zhu, Z., Xiong, C., Chen, R., Xu, W., Qiao, H., Peng, W., Nie, Z., Chen, Y.: Characteristics of stability boundary and frequency in nonlinear ion trap mass spectrometer. J. Am. Soc. Mass Spectrom. **21**, 1588–1595 (2010)
18. Zhou, X., Xiong, C., Xu, G., Liu, H., Tang, Y., Zhu, Z., Chen, R., Qiao, H., Tseng, Y., Peng, W., Nie, Z., Chen, Y.: Potential distribution and transmission characteristics in a curved quadrupole ion guide. J. Am. Soc. Mass Spectrom. **22**, 386–398 (2011)
19. Dehmelt, H.G., Bates, D.R., Immanuel, E.: Radiofrequency spectroscopy of stored ions. I: storage. Adv. At. Mol. Phys. **3**, 53–72 (1968)
20. Gao, C., Douglas, D.J.: Can the effective potential of a linear quadrupole be extended to values of the Mathieu parameter q up to 0.90? J. Am. Soc. Mass Spectrom. **24**, 1848–1852 (2013)
21. Doroudi, A.: Calculation of coupled secular oscillation frequencies and axial secular frequency in a nonlinear ion trap by a homotopy method. Phys. Rev. E **80**, 056603 (2009)
22. Doroudi, A.: Comparison of calculated axial secular frequencies in nonlinear ion trap by homotopy method with the exact results and the results of Lindstedt-Poincare approximation. Int. J. Mass Spectrom. **296**, 43–46 (2010)
23. Doroudi, A., Asl, A.R.: Calculation of secular axial frequencies in a nonlinear ion trap with hexapole, octopole and decapole superpositions by a modified Lindstedt-Poincare method. Int. J. Mass Spectrom. **309**, 104–108 (2012)
24. Sevugarajan, S., Menon, A.G.: Field imperfection induced axial secular frequency shifts in nonlinear ion traps. Int. J. Mass Spectrom. **189**, 53–61 (1999)
25. Sevugarajan, S., Menon, A.G.: Transition curves and iso-$\beta_u$ lines in nonlinear Paul traps. Int. J. Mass Spectrom. **218**, 181–196 (2002)
26. Zhao, X., Granot, O., Douglas, D.J.: Quadrupole excitation of ions in linear quadrupole ion traps with added octopole fields. J. Am. Soc. Mass Spectrom. **19**, 510–519 (2008)
27. Wang, Y., Huang, Z., Jiang, Y., Xiong, X., Deng, Y., Fang, X., Xu, W.: The coupling effects of hexapole and octopole fields in quadrupole ion traps: a theoretical study. J. Mass Spectrom. **48**, 937–944 (2013)
28. Guo, D., Wang, Y., Xiong, X., Zhang, H., Zhang, X., Yuan, T., Fang, X., Xu, W.: Space charge induced nonlinear effects in quadrupole ion traps. J. Am. Soc. Mass Spectrom. **25**, 498–508 (2014)
29. Guidugli, F., Traldi, P.: A phenomenological description of a black hole for collisionally induced decomposition products in ion-trap mass spectrometry. Rapid Commun. Mass Spectrom. **5**, 343–348 (1991)
30. Williams, S., Siu, K.W.M., Londry, F., Baranov, V.: Study of the enhancement of dipolar resonant excitation by linear ion trap simulations. J. Am. Soc. Mass Spectrom. **18**, 578–587 (2007)
31. Du, Z., Douglas, D.J., Konenkov, N.: Peak splitting with a quadrupole mass filter operated in the second stability region. J. Am. Soc. Mass Spectrom. **10**, 1263–1270 (1999)
32. Xiong, C., Zhou, X., Zhang, N., Zhan, L., Chen, S., Nie, Z.: Nonlinear effects in Paul traps operated in the second stability region: analytical analysis and numerical verification. J. Am. Soc. Mass Spectrom. **25**, 1882–1889 (2014)
33. Press, W.H., Teukolsky, S.A., Vetterling, W.T., Flannery, B.P.: Press syndicate of the University of Cambridge (2nd ed.): New York (1992)
34. Zhao, X., Douglas, D.J.: Dipole excitation of ions in linear radio frequency quadrupole ion traps with added multipole fields. Int. J. Mass Spectrom. **275**, 91–103 (2008)